International Journal of Heat and Mass Transfer 132 (2019) 52–67

Contents lists available at ScienceDirect

International Journal of Heat and Mass Transfer

journal homepage: www.elsevier.com/locate/ijhmt

Dropwise condensation heat transfer on superhydrophilic-hydrophobic network hybrid surface

Xianbing Ji, Dongdong Zhou, Chao Dai, Jinliang Xu *

The Beijing Key Laboratory of Multiphase Flow and Heat Transfer, North China Electric Power University, Beijing 102206, PR China

ARTICLE INFO

Article history:
Received 2 April 2018
Received in revised form 30 October 2018
Accepted 27 November 2018

Keywords:
Superhydrophilic groove
Network
Hybrid surface
Wettability
Condensation heat transfer

ABSTRACT

Superhydrophilic-hydrophobic (SHPi-HPo) network hybrid surface was designed to investigate the condensation heat transfer using stainless steel as substrate material. The SHPi-HPo surface was comprised of superhydrophilic network grooves and hydrophobic regions. Hydrophobic (HPo) surface was prepared with fluorocarbon coating using polytetrafluoroethylene (PTFE) as the matrix resin and micro-nano silicon dioxide (SiO_2) as additive to control surface roughness. Three kinds of SHPi-HPo surfaces were tested, having a grid spacing of 1.5, 2.5 and 3.5 mm and named as SHPi-HPo-1, SHPi-HPo-2 and SHPi-HPo-3, respectively. To study the effects of the wall subcooling, steam mass flux, cooling water temperature, cooling water mass flow rate and grid spacing, a series of experiments were conducted and a high speed camera was used to visualize the condensation process. The results show that SHPi-HPo surface can well control condensate droplet diameters and its condensation heat transfer performance is better than that of smooth hydrophilic (HPi) and HPo surfaces. This is attributed to SHPi-HPo surface sucking away droplets in time and limiting the growth of large condensate droplets through the superhydrophilic grooves. At wall subcooling $\Delta T_w = 6.3$ K, the heat transfer coefficient of SHPi-HPo-2 surface is 2.7 and 3.4 times that of HPi and HPo surfaces, respectively. For SHPi-HPo surface, there is optimum grid spacing between superhydrophilic grooves to enhance condensation heat transfer. Among three SHPi-HPo surfaces, the heat transfer coefficient of SHPi-HPo-2 surface has the best condensation heat transfer performance, about 0–10% higher than that of SHPi-HPo-1 surface, and at $\Delta T_w = 9$ K, the heat transfer coefficient is 1.7 times that of SHPi-HPo-3 surface.

1. Introduction

Condensation heat transfer is a phase-change phenomenon, which is widely used in the industrial processes, such as power generation [1], chemical production [2], thermal management [3], nuclear safety [4] and other fields [5]. Therefore enhancing condensation heat transfer coefficient is an important research field. According to whether the solid surface can be wetted by the liquid phase, steam condensation can be divided into two types: filmwise condensation and dropwise condensation [6]. For filmwise condensation, a liquid film covers the solid surface, resulting in a high thermal resistance between the steam and condensation surface [7]. For dropwise condensation, the steam condensation occurs on the surfaces in forms of liquid droplets. Compared to filmwise condensation, dropwise condensation is characterized by larger heat transfer coefficient [8].

Since 1930, Schmidt et al. [9] discovered the dropwise condensation heat transfer. Many researchers have done a lot of researches on it. These studies can be found in literatures [10,11]. Some researchers [12,13] considered that the superhydrophobic surface had a good heat transfer performance, while some researchers [14,15] have reported reduced condensation heat transfer coefficients on the superhydrophobic surfaces with microscale and nanoscale surface structures compared to hydrophobic surfaces. Hwang et al. [16] even gave a suggestion that the superhydrophobic surface was not suitable to enhance condensation heat transfer in intensive condensing devices. The other scholars also had the same results, for example, Lee et al. [17] found that due to the existence of extra thermal resistance of covers prepared by the polymer and self-assembled layer film, dropwise condensation heat transfer coefficients occurred on this hydrophobic surface was smaller than that of filmwise condensation. Why are there these different conclusions above?

In fact, dropwise condensation is a dynamic cycle process accompanied by droplet nucleation, growth, merging and detachment, where droplet detachment is not only the end of a cycle,

* Corresponding author.
E-mail address: xjl@ncepu.edu.cn (J. Xu).

https://doi.org/10.1016/j.ijheatmasstransfer.2018.11.139
0017-9310/

Nomenclature

A	cooling area, m^2
Bo	Bond Number
C	constant
CA	contact angle, °
D	hydraulic diameter, m
d	grid spacing, m or droplet diameter, mm
c_p	constant-pressure specific heat, J/kg·K
ΔT_c	inlet and outlet temperature difference of cooling water, K
ΔT_w	wall subcooling, K
F_f	friction force, N
F_n	support force, N
F_u	adhesive force, N
G	mass flux, kg/(m^2·s)
g	gravity, m/s^2
H_L	$H_L = HTC_{Nu}(T_{sat} - T_w)l/r_{lv}$
HTC	heat transfer coefficient, W/(m^2·K)
L	distance between two temperature measurement points, m
L_o	distance between condensation surface and temperature measurement point, m
l	length of the liquid film, m
m	mass flow rate, kg/h
q	heat flux, W/m^2
R	droplet diameter, m
r_{lg}	latent heat of vaporization, J/kg
T	temperature, °C
t	time, s
dT/dx	temperature gradient, K/m
dp/dz	two-phase frictional pressure gradient, Pa/m

Greek symbols

β	function of contact angle
ρ	density, kg/m^3
λ	thermal conductivity, W/(m·K)
μ	dynamic viscosity, Pa·s
θ_A	advancing angle
θ_R	receding contact angle
σ	surface tension
θ	static contact angle

Subscript

c	cooling water
c, in	cooling water inlet
g	gas
l	liquid
m	mean particle
Nu	Nusselt theory
s	steam
sat	saturation
SS	shear stress
s, in	steam inlet
t	total
w	wall
1–11	temperature measurement point

but also prepare a blank surface for the next droplet nucleation and growth, which plays an important role in dropwise condensation. Many researchers found that large droplets have a large thermal resistance and small droplets are beneficial to the heat transfer in droplet condensation process [18]. The lag of droplet detachment from the surface will greatly delay the renewal of the surface and thereby reduce the effective heat transfer area and seriously affect the condensation heat transfer [19]. Therefore, how to reduce the droplet diameter and promote the droplet detachment in time is the key to strengthen condensation heat transfer [20]. For this purpose, domestic and foreign researchers have done a lot of work [21]. According to different driving forces, there are three methods to do this: (1) inhomogeneous wettability surface, (2) droplets jumping, (3) sweeping of falling droplet. The details are as follows:

(1) **Inhomogeneous wettability surface**: Chaudhury and Whitesides [22] reported the droplet movement on a gradient wetting surface for the first time in the Journal of Science. Zhu et al. [23] observed that droplet movement speed was up to 42 mm/s on the horizontal gradient wettability surface. They analyzed droplet movement from the point of view of the surface free energy, and pointed out that the main reason for the droplet movement is interfacial energy transformation in the droplet deformation process. Chen et al. [18] showed that by harnessing inhomogeneous wettability and hierarchical roughness features in multiscale structures, they can enhance both droplet nucleation and departure on a condensation surface, allowing for ~65% increase in the droplet number density and ~50% increase in the droplet self-removal volume as compared to a superhydrophobic surface with nanostructures alone. Macner et al. [24] found that the combination of droplets can drive droplets to migrate from a weakly wetting area to a strong wetting area, and this rapid droplet spontaneous migration can change the size distribution of the droplet and enhance the heat transfer performance. It is worth noting that literatures [25] studied the condensation heat transfer on hydrophilic/hydrophobic surfaces, and found that the combination of the hydrophilic/hydrophobic surfaces was favorable for the droplet detachment. Recently, Guo and Cheng [26] have well explained why hybrid wettability is conducive to condensation heat transfer from the perspective of condensation nucleation, using a newly developed 3D multi-component multiphase lattice Boltzmann model, and found three preferred nucleation sites with different surface wettability contrasts.

(2) **Droplet jumping:** Boreyko and Chen [27] first reported the phenomenon of two small droplets merging into a large droplet and jumping from the surface in 2009. Then Feng et al. [28] studied droplet behaviors on different surfaces, they thought condensate droplets moving along surface or bouncing behavior related to surface structure parameters. These parameters influence the wetting state of condensed droplets, while Cassie state is a key factor determining whether the two droplets are bounced after the combination. Peng et al. [29] calculated the bouncing velocity and jumping height induced by droplet coalescence, basing on the energy conservation. Leach et al. [30] performed a series of experiments and simulations, found that droplet coalescence plays a critical role in determining the drop-size distribution and stimulates the nucleation of new, small droplets on the substrates, and the rate of condensation per unit substrate area is especially high for the smallest drops and may help account for the high heat transfer rates associated with dropwise condensation. Recently, Chu et al.

[31] numerically simulated the droplet jumping process. The results show that increasing the coalesced droplet number was advantageous for surface energy releasing and concentrated droplet distribution was conductive to increase the energy conversion efficiency from the surface energy to the jumping energy.

(3) **Sweeping of falling droplet:** It is an important method for strengthening condensation heat transfer to rapidly remove condensate droplets from the surface. Yamali and Merte [32] put the condensation surface on the centrifuge and carried out dropwise condensation experiments. The results showed that the condensation heat transfer coefficient increases with an increase in body force, indicating that the sweeping of droplets are beneficial to the condensation heat transfer. Yamali and Merte [33] studied the sweeping effects of the droplets on the heat transfer performance under atmospheric pressure. As the wall subcooling was low, the sweeping effect of droplets was conducive to the heat transfer. However, the condensation heat transfer was worsened at high wall subcooling. Izumi et al. [34] vertically placed the condensation surface and carved circular grooves on it. When the steam was condensed on the condensation surface, the droplets will slide down the groove and take away the droplets below. Lee et al. [35] also thought that the sweeping of falling droplet on the vertical wall can remove the small droplets attached to the wall, which is beneficial to the condensation heat transfer.

Although inhomogeneous wettability surface, droplets jumping and sweeping of falling droplet have been investigated, for most of dropwise condensation researches above, the test surfaces are small and mostly made of copper, aluminum and silicon, there is a lack of systematic experimental data in using stainless steel as material to investigate droplet condensation on a large area surface [36]. However, stainless steel is the most common material in the industrial condensation. Therefore, it is of great industrial application value to study droplet condensation heat transfer on large area stainless steel surface with strong resistance to the scour of high temperature steam. Some animals and plants in the nature provide good ideas to solve this problem, for example, on the back of beetle living in the desert, there are mastoid surfaces with wax nano structure to capture moisture in the air and micro grooves with hydrophobic property to easily transport liquid [37]. Cactus collects the water in the fog through this principle called functional synergy [38]. Therefore, in this paper we prepared superhydrophilic-hydrophobic (SHPi-HPo) network hybrid surfaces to study condensation heat transfer. Superhydrophilic network grooves were carved on the hydrophobic (HPo) surface prepared with fluorocarbon coating using polytetrafluoroethylene (PTFE) as the matrix resin and micro-nano silicon dioxide (SiO_2) as additive to control surface roughness. This paper chooses stainless steel as substrate materials to do dropwise condensation heat transfer experiments on superhydrophilic-hydrophobic network hybrid surface based on the following points: (1) At present, the study of dropwise condensation heat transfer is mainly concentrated on the copper, aluminum and silicon surface. However, stainless steel has become one of the most widely used materials in the world because of its low price and reliable performance. Many large heat exchangers, such as containment in nuclear power plant, condenser in power plant and other important parts are all made of stainless steel. (2) PTFE with SiO_2 as additive has a strong adhesion to stainless steel surface (much better than copper and aluminum). (3) The thermal conductivity of stainless steel is much lower than that of copper and aluminum, so the thin PTFE thermal resistance has little effect on the condensation heat transfer. (4) Dropwise condensation heat transfer experiment on large area stainless steel surface is more realistic, considering the inertia force and scouring effect of droplets. In addition, micro-nano SiO_2 was used as additive to adjust the surface roughness and increase condensation area. Based on above description, this study is unique.

2. Experimental setup and test section

2.1. Experimental setup

The experimental setup is shown schematically in Fig. 1. The system mainly consists of four components: a steam generator, a test section, a post-condenser and cooling water loops. Steam is generated in a cylindrical steam generator which has a rated power of 18 kW and is connected to the test section by a steam pipe. The pressure of saturated steam is controlled by the pressure controller carried by the boiler itself. To avoid steam condensation before entering the test section, the connection pipes between the generator and the test section are insulated using high thermal insulation material and heated by an electric resistance wire installed around the pipe. The steam pipe is made of stainless steel and a T-type thermocouple was used to monitor wall temperature. The steam mass flux can be controlled by the regulating valve at the outlet of the generator, and is measured by the orifice flowmeter between the generator and test section, in range of 0–4.5 kg/(m^2·s). At the inlet and outlet of steam chamber (a part of test section where most of steam is condensed), a pressure transducer and a K-type thermocouple was used to measure the pressure and temperature of steam, respectively. Downstream the test section, two-phase mixture passes through a post-condenser where the steam is condensed completely. The post-condenser consists of a cylinder containing and a coiled tube. The steam condenses on the external surface of the coiled tube, while the cooling water flows inside the tube. To measure the quality of condensate liquid, the condensate liquid flows into the container placed on an electronic balance with an accuracy of 0.02 g. For cooling water loops, a cooling water nozzle is installed on the upper part of cooling chamber. Cooling water sprays on the surface of vertical test plate and forms a water film to take away heat from steam condensation. Except a small portion of the heat taken away by the post-condenser, most of them are taken away by the cooling water in the cooling chamber. The inlet and outlet temperatures of cooling water are measured by T-type thermocouples. After coming out of cooling chamber, the water is cooled by an air cooling unit, and then pumped into the constant temperature unit to control the cooling water temperature, at last flows into cooling chamber and completes a cycle. A mass flowmeter with a range of 0–120 kg/h was used to measure cooling water mass flow rate. Finally, after the construction of experimental setup, the pipes and test section were insulated to avoid heat losses to the ambient. Because a small amount of non-condensable gas has a great effect on the condensation heat transfer, the system was vacuumed by a vacuum pump. Firstly, distilled water is added into the steam generator (boiler) and pumped by water ring vacuum pump. When the system pressure reaches steam pressure at room temperature, the boiler is opened and make distilled water circulate for evaporation and condensation about 1 h and also preheat the test section. Then boiler outlet valve is closed and non-condensable gas accumulated in the condensation chamber and post-condenser is pumped by water ring vacuum pump. When the residual water is drained, open the vacuum pump and pump the system pressure to less than 0.5 ± 0.1 Pa. In the whole heat transfer test, the temperature and pressure of the steam in the condenser are monitored, and non-condensable gas content of the system is calculated by the gas partial pressure law. When non-condensable gas exists in the system, the

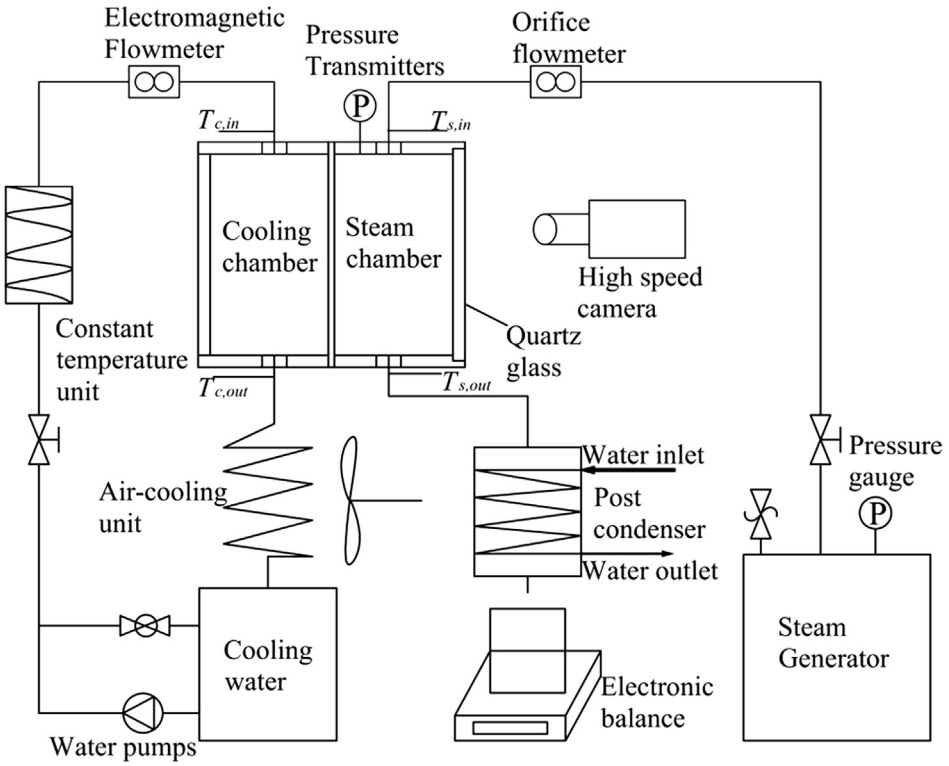

Fig. 1. Schematic diagram of experimental setup.

experiment is stopped. When non-condensable gas is completely eliminated again, the experiment is reopened to ensure that the experiment is carried out in pure steam environment. Besides, a high speed camera was used to visualize the droplet condensation process. Fig. 2 shows the picture of experimental apparatus.

2.2. Test section

Fig. 3 shows the test section (easily visualizing the condensation process). It consists of a stainless steel condensation board (test plate), high thermal insulation frames and quartz glasses. Its overall shape is a vertical rectangular body with a size of 60 × 240 mm (see Fig. 3a). As shown in Fig. 3b, the test plate has a thickness of 5.0 mm and the dimensions of condensation surface are 40 × 220 mm. The test plate divides the test section into steam chamber and cooling chamber. On one side of the test plate, the steam passes through the steam chamber from top to bottom and condenses on the test condensation surface. On another side, the cooling water flow along test plate surface. One side of steam chamber near the outside environment is covered by double quartz glasses to allow the visualization of condensation process. To remove the droplets condensed on the glass surface for better observation of steam condensation, the double glasses were designed with an air chamber for thermal insulation. The frontal glass can be heated by 10 electrical heaters with a power of 10 W. Except observation window and condensation surface, the other surfaces are covered by high temperature insulation materials, so most of steam coming from the steam generator is condensed on the condensation surface. The distribution of steam temperature measurement points (1–3) and cooling water temperature measurement points (4–5) can be found in Fig. 3a. To calculate heat flux, wall subcooling and condensation heat transfer coefficient, six K-type thermocouples (6–11) with a diameter of 0.2 mm are arranged inside the test plate and the depth of temperature measurement point from the surface is 0.5 mm (see Fig. 3c). Thermocouples need to be aligned perpendicular to expected isotherms. To decrease contact resistance, thermocouples buried method invented by Xie et al. [39] was adopted, as shown in Fig. 3d. Initially, a hammer hit the point chisel on the stainless steel plate wall to lift a thin steel film from the plate wall. The thermocouple wire was buried in the cavity beneath the steel film. Finally, the hammer hit the blunt chisel on the steel film to tightly populate the thermocouple wire in the cavity. This method can greatly reduce the contact thermal resistance, even the effect of contact thermal resistance was negligible.

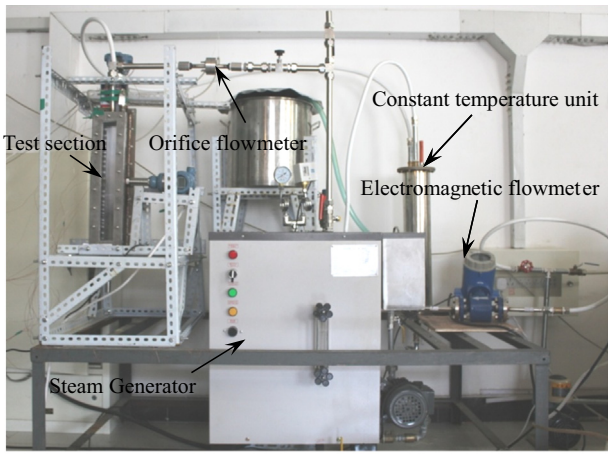

Fig. 2. Picture of experimental apparatus.

2.3. Data reduction and uncertainty analysis

To obtain condensation heat flux, we regard the heat transfer in the test plate as one-dimensional heat conduction. Therefore, we get the heat flux according to following formula:

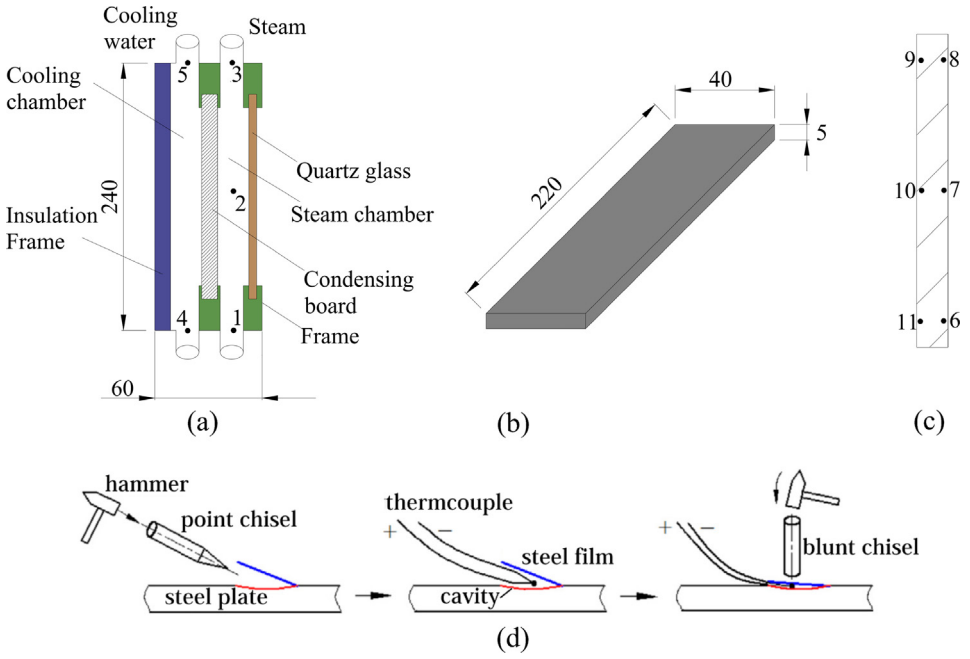

Fig. 3. Test section: (a) structure composition and distribution of temperature measurement points, (b) test plate, (c) location of the thermocouples inside the test plate, (d) thermocouples buried in the stainless steel plate cavity [39].

$$q_w = -\lambda\frac{dT}{dx} = \lambda\frac{(T_6+T_7+T_8)-(T_9+T_{10}+T_{11})}{3L} \tag{1}$$

where λ is the thermal conductivity of stainless steel, dT/dx is the temperature gradient along thickness direction of the test plate, L is the linear distance between two temperature measurement points on both sides of plate, such as the distance between the temperature measurement points 6 and 11 (see Fig. 3c). $T_{6\text{-}11}$ are the corresponding temperature measurement values.

At the same time, the heat flux obtained by formula (1) will be checked by the heat flux q_1 obtained by the inlet and outlet temperature difference of cooling water:

$$q_1 = \frac{m_c c_p \Delta T_c}{A} \tag{2}$$

where m_c, c_p and ΔT_c are the mass flow rate, specific heat and inlet and outlet temperature difference of cooling water, respectively, A is the cooling area. In present experiments, strict insulation measures were adopted for the test parts and heat leakage is very small. The results show that heat flux obtained from the inlet and outlet temperature difference of cooling water is slightly less than that obtained by Fourier law. The maximum difference between them is only 1.6%. Compared to copper, small thermal conductivity of stainless steel will result in large temperature gradients at the same heat flux. For small and thick stainless steel, the system may not be truly following one-dimensional heat conduction inside the substrate. However, our condensation plate is relatively large and thin, the length and width are much larger than the thickness, and surrounding materials are high-temperature insulation materials. Thus, it can be regarded as an infinite plate and considered as one-dimensional thermal conductivity. Corresponding surface temperature at three locations can be calculated from the following formula:

$$T_{w1} = T_6 + \frac{(T_6-T_{11})L_o}{L}, T_{w2} = T_7 + \frac{(T_7-T_{10})L_o}{L}, T_{w3} = T_8 + \frac{(T_8-T_9)L_o}{L} \tag{3}$$

where L_o is the distance between condensation surface and temperature measurement point 6–8. So the average wall subcooling is:

$$\Delta T_w = \frac{(T_1-T_{w1})+(T_2-T_{w2})+(T_3-T_{w3})}{3} \tag{4}$$

where $T_{1\text{–}3}$ are the saturation temperature of steam at temperature measurement points 1–3. The maximum temperature difference is 1.4 K among three different locations (some cases can be seen in Table 2). In evaluation of uncertainty analysis, the variations of the wall temperature need to be fully considered. Finally, the condensation heat transfer coefficient (HTC) is evaluated as below:

$$HTC = \frac{q}{\Delta T_w} \tag{5}$$

The mass flow rates of steam and cooling water are measured by an orifice flowmeter and an electromagnetic flowmeter, respectively. To calibrate flowmeters, an electronic balance with an accuracy of 0.02 g was used to get the relationship between mass flow rate and voltage signal. The temperature measurement has a maximum uncertainty of 0.2 K, and the pressure and pressure drop measurements have accuracies of 0.1%. To get reasonable error analysis, the variation of wall temperature at three locations and the random error induced by the radius of holes for installing thermocouples need to be considered in the uncertainties analysis. Within the present experiment range, the maximum uncertainties of heat flux and the condensation heat transfer coefficient are 8.17% and 9.4%, respectively.

3. Results and discussion

3.1. Preparation and characterization of test surface

First of all, we prepared a smooth hydrophilic (HPi) surface for the comparison test (see Fig. 4a). The HPi surface was obtained by grinding the stainless steel surface successively with 200 and 5000 mesh sandpapers. To prepare HPo surfaces, stainless steel surfaces were firstly polished with 220 and 600 mesh sandpapers, then HCl solution with a ratio of 3:1 was used to corrode the stainless steel surfaces for 1 min, next surfaces were cleaned in deionized water. In the spraying process, the fluorocarbon coating was diluted by the cyclohexanone solution with a ratio of 1:2. After dilution,

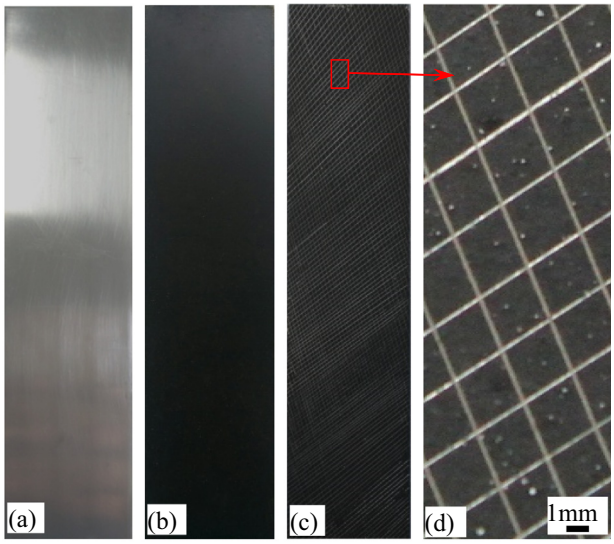

Fig. 4. Pictures of three test plates ((a) HPi surface, (b) HPo surface, (c and d) SHPi-HPo-2 surfaces).

fluorocarbon coating was added 0.1 g micron and nano silica particles, respectively. A spray gun with an aperture of 1.2 mm was used to spray fluorocarbon coating on the stainless steel surfaces. Finally the sprayed stainless steel test plates were put into the oven and baked for 10 min at 320 °C. So the fluorocarbon coating layer was formed on the surfaces and HPo surfaces were achieved (see Fig. 4b). To get SHPi-HPo surfaces, network grooves with a width of 0.4 mm and a depth of 0.5 mm were carved on the HPo surface by machining methods. Then we immersed the test plate in 30% hydrogen peroxide solution for 8 h and got superhydrophilic network grooves on HPo surfaces. There are three kinds of SHPi-HPo surfaces, having grid spacing (the distance between two adjacent grooves) of 1.5, 2.5 and 3.5 mm, being named as SHPi-HPo-1, SHPi-HPo-2 and SHPi-HPo-3, respectively (see Table 1). SHPi-HPo-2 surface can be seen in Fig. 4c. Fig. 4d is a local large map of Fig. 4c.

For test surfaces, their surface wettabilities and structures can be characterized by the contact angle and Scanning Electron Microscopy (SEM) images. Fig. 5a and b show the SEM images of HPi surface. This smooth surface has small roughness and there are not any other large structures except for ~1 mm wide grooves. Therefore, stainless steel surface grinded by sand paper is hydrophilic, and its static contact angle (CA) is 62°. However, as shown in Fig. 5c–e, HPo surface is coated by fluorocarbon coating with micro and nano silica particles. On this surface, big micro particles have a diameter of about 73 μm (Fig. 5c), and there are submicron particles of ~4.5 μm on them (Fig. 5d). In Fig. 5e, magnification image shows that the submicron particles are fully covered by nano particles with a diameter of 45 nm. These structures make the HPo surface have micro-nano hierarchical roughness. Duo to low density micro particles, this surface is unable to reach superhydrophobic state and only has hydrophobic characteristics. Its CA is up to 132°. Since the droplets move, the dynamic contact angle is important for dropwise condensation phenomena. So rolling angle (RA), advancing contact angle (θ_A) and receding contact angle (θ_R) were also measured by contact angle measurement instrument and they were 22.5°, 124.5° and 102°, respectively (see Fig. 5d). This hydrophobic surface on stainless steel, similar to the surface of non-stick pot, has strong hardness, friction resistance and high temperature scouring resistance. Therefore, dropwise condensation can continued during whole period of experiments and dropwise condensation did not converted to film condensation. However, the strength of superhydrophilic structures in the groove is not strong. Fortunately, the superhydrophilic structures are in grooves, it is difficult to directly wash the superhydrophilic surface by steam and liquid. The superhydrophilic groove has little damage in one test. Only after many tests, the superhydrophilicity began to decrease, and the condensation heat transfer will be affected.

Fig. 5f–h show the SEM images of superhydrophilic grooves. The surface is covered with ribbed structure and the distance between two ribs is about 0.4 μm. On the ribbed structures, there are nano structures with a size of 45 nm. These structures make the grooves have certain roughness and have superhydrophilic characteristics. The CA is only about 3°.

Fig. 6 presents AFM images for smooth surface and hydrophobic surface. Fig. 6a is an AFM diagram for smooth surface, including 3D, 2D and cross-sectional height curves. It is found that the surface roughness is small in the scanning range of 5 × 5 μm, the average roughness (*Ra*) is only 17.901 nm, the root mean square roughness (*RMS*) is 57.820 nm. The maximum vertical height difference on the cross-sectional surface is 142.10 nm. Fig. 6b is the AFM diagram of hydrophobic surface. From three sub-graphs, it is found that the surface roughness is large in the scanning range of 5 × 5 μm. *Ra* and *RMS* reach 43.554 nm and 369.49 nm which are 2.43 and 6.39 times that of smooth surface, respectively. The maximum vertical height difference on the cross-section is 1.053 μm. The surface roughness is obviously increased. We know that the

Table 1
Five test surfaces.

Surface name	Wettability	Grid spacing (mm)	Groove depth (mm)	Groove width (mm)
HPi	Hydrophilic	\	\	\
HPo	Hydrophobic	\	\	\
SHPi-HPo-1	Superhydrophilic + hydrophobic	1.5	0.5	0.4
SHPi-HPo-2	Superhydrophilic + hydrophobic	2.5	0.5	0.4
SHPi-HPo-3	Superhydrophilic + hydrophobic	3.5	0.5	0.4

Table 2
Temperature difference between upper, middle and lower wall surfaces under three cooling water mass flow rates ($G_{s,in}$ = 3.17 kg/m^2 s).

Cooling water flow rate (kg/h)	T_{w1} (°C)	T_{w2} (°C)	T_{w3} (°C)	$(T_{w1} + T_{w2} + T_{w3})/3$ (°C)	Maximum temperature difference (K)
26.4	100.0	99.2	98.6	99.3	1.4
42.7	93.0	93.2	94.3	93.5	1.3
61.2	89.7	90.4	90.9	90.3	1.2

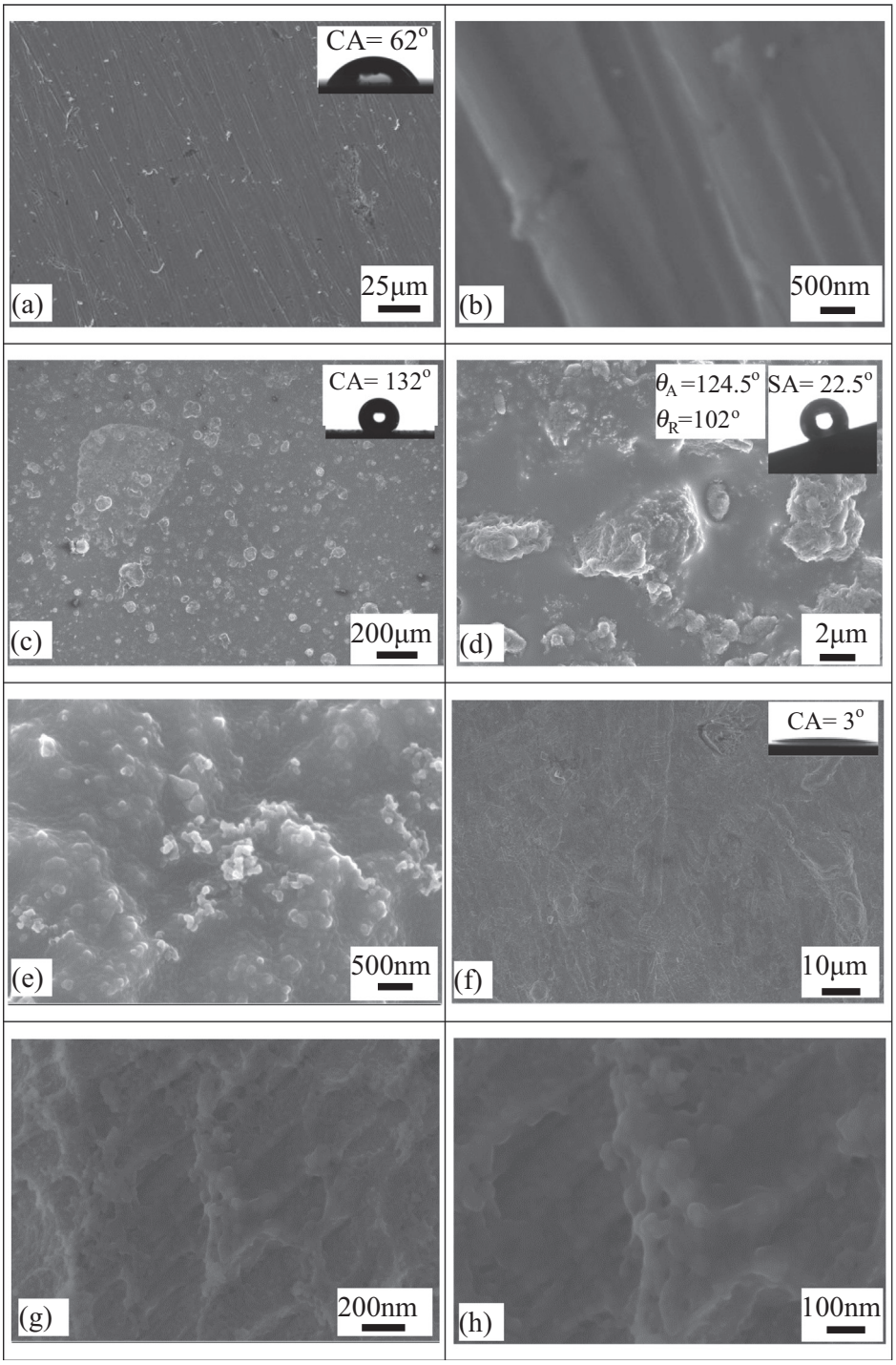

Fig. 5. SEM images of three wettability surface ((a and b) HPi surface, (c–e) HPo surface, (f–h) superhydrophilic grooves).

formation of hydrophobic surfaces depends on the polymerization energy between molecules and the surface roughness. According to the Wenzel model, for a hydrophobic surface, the surface wettability can be enhanced by increasing surface roughness. Therefore, we improve surface hydrophobicity by adding nano-silica in the PTFE to increase surface roughness. The surface static contact angle and rolling angle can reach 132° and 22.5°, respectively. However, the hydrophobicity enhancement is the results of the interaction of surface energy and roughness, so it is difficult to eliminate the effect of roughness on dropwise condensation heat transfer. Fortunately, the main purpose of our paper is to study the heat transfer improvement of hybrid surface relative to the hydrophobic surface. Smooth surface is only a reference, the hybrid surface was only formed by preparing some superhydrophilic grooves on the hydrophobic surface, and the groove width is very small, so the effect of roughness on the comparison between hybrid and hydrophobic surface is not significant.

3.2. Reliability verification

To verify the reliability of experiments, a filmwise condensation on HPi surface was conducted. In present experiments, because of

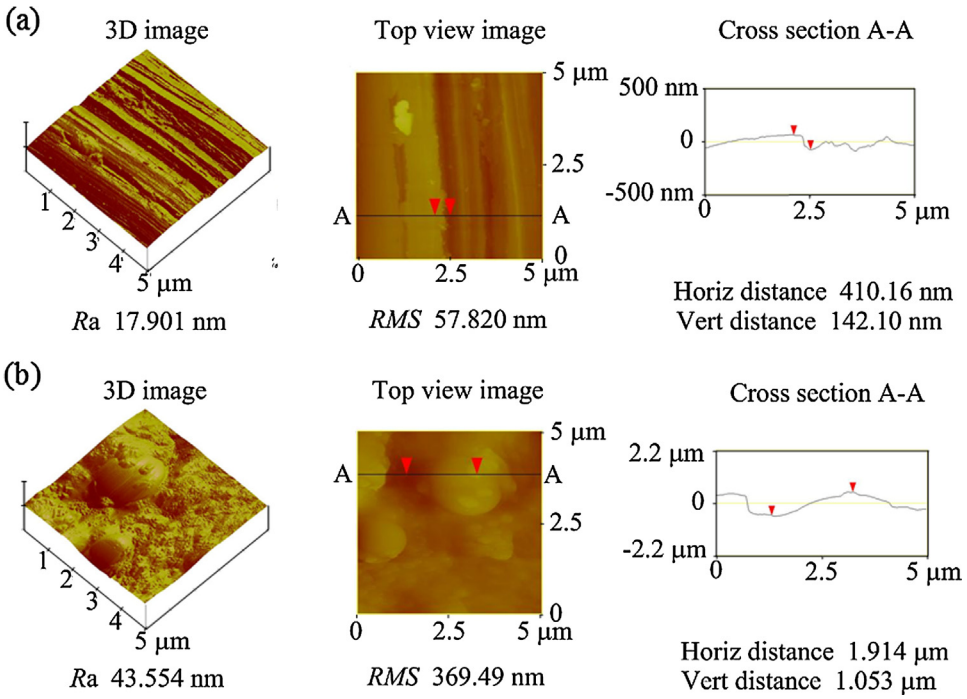

Fig. 6. AFM images ((a) for smooth surface, (b) for hydrophobic surface).

the same directions of the steam flow, liquid film flow and gravity, we must consider the effects of the gravity and shear force on the gas-liquid interface. For gravity-controlled condensation over vertical plain surfaces, the *HTC* can be predicted using a corrected formula of the Nusselt film theory [40,41]:

$$HTC_{Nu} = 1.15 \cdot \left[0.0206\left(\frac{r_{lg}\mu_l}{\lambda_l(T_{sat}-T_w)}\right)^{1/2} + 0.79\right] \cdot 0.943 \cdot \left[\frac{\rho_l(\rho_l-\rho_v)gr_{lg}\lambda_l^3}{\mu_l(T_{sat}-T_w)l}\right]^{1/4} \quad (6)$$

where λ_1, μ_l and ρ_l are the thermal conductivity, dynamic viscosity and density of condensate water, respectively, ρ_g is the steam density, g is the gravity acceleration, r_{lg} is the latent heat of vaporization, l is the length of liquid film along gravity direction, T_{sat} and T_w are the saturation steam temperature and surface temperature, respectively. Considering the effect of interfacial shear stress, we used the shear stress correlation proposed in the literature [42]. The corresponding two-phase heat transfer coefficient can be calculated as:

$$HTC_{SS} = \sqrt{\frac{\lambda_l^2\rho_l D}{8H_L\mu_l}\left(\frac{dp}{dz}\right)} \quad (7)$$

where $H_L = HTC_{Nu}(T_{sat} - T_w)l/r_{lg}$, D is the hydraulic diameter of the condensation channel and dp/dz is the two-phase frictional pressure gradient. When condensation occurs under the combination effects of gravity and shear force, as in the present case, the total heat transfer coefficient can be calculated [40,41]:

$$HTC_t = \sqrt{HTC_{Nu}^2 + HTC_{SS}^2} \quad (8)$$

Fig. 7 indicates that the heat transfer coefficient decreases with increasing wall subcooling, and the deviation between the experimental data and modified Nusselt model is within 10%. Therefore, it is credible that the methods of parameter measurements and data processing in present experiments. However, there is a clear

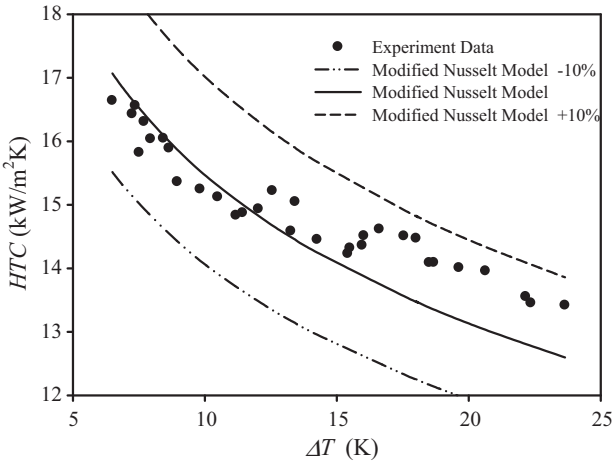

Fig. 7. Comparison of filmwise condensation heat transfer coefficients between experimental and theoretical results.

difference between the experimental data when wall subcooling is lower versus when the wall subcooling is higher. When wall subcooling is lower, the data fall below the modified Nusselt model, and vice versa. The main reason is the influence of inertia force. In modified Nusselt model, the effect of inertia force on droplet behavior is not considered. In fact the inertia force has important influence on the condensation heat transfer, when the condensation plate area is larger in height direction as well as our present experiments. As the subcooling is higher, the downward inertia force of liquid film is larger, the liquid film located at the top wall will have a certain scouring effect on the liquid on the bottom wall, which promote liquid move and detach from wall. Therefore, with increasing wall subcooling, the scouring effect is more obvious, and heat transfer coefficient obtained from experiments is naturally larger than that obtained from modified Nusselt model. When wall subcooling is lower, the inertia force is small which has a little

influence on the liquid film behavior. So experiment data is close to the model calculation value. Of course, the instability of cooling water temperature will result in fluctuation of heat transfer, especially for lower wall subcooling. Small fluctuations of wall subcooling will lead to large variations in heat transfer coefficients, so the number of experimental repetitions should be increased in this situation. Some repeated experiment data are shown in Fig. 7.

3.3. Effects of steam mass fluxes

Seven steam mass fluxes ($G_{s,in}$) were selected in range of 0–4.5 kg/m^2 s under the specific cooling water mass flow rate and temperature. The choice of mass-flux (G_s) range needs to fully consider the influence of condensation area. When the mass fluxes are less than 0.5 kg/m^2 s, there may be a shortage of steam. In order to ensure uniform condensation on the plate surface, we use 0.5 kg/m^2 s as the lower limit of mass fluxes. When the mass-flux is too larger, the scouring force of steam flow is larger, and some steam may be taken away by the steam flow before the steam condensation is completed. To avoid inadequate condensation of steam, excessive steam flow rate was controlled and the upper limit of mass fluxes is 4.5 kg/m^2 s. The effects of steam mass flux on the condensation heat transfer were studied for three wettability surfaces. Fig. 8a shows the *HTC* increases with increasing steam mass fluxes at the mass flow rate $m_{c,in}$ = 101.4 kg/h and cooling water temperature $T_{c,in}$ = 30 °C for three surfaces. However, The SHPi-HPo-2 surface has the maximum *HTC* among three surfaces. The *HTC* of HPo surface increases slowly with increasing steam mass fluxes. As $G_{s,in}$ > 2.5 kg/m^2 s, the *HTC* of both HPo and HPi surfaces tend to be a stable value. However, as $G_{s,in}$ < 2.0 kg/m^2 s, the *HTC* of HPo surface is higher than that of HPi surface. Fig. 8b shows the relationship between the heat flux and steam mass fluxes for three surfaces. The heat fluxes increase slowly with increasing steam mass fluxes. As $G_{s,in}$ > 3.0 kg/m^2 s, the heat fluxes tend to be a stable value. For the same steam mass flux, the SHPi-HPo surface has the maximum heat flux and HPo surface has the minimum heat flux. As $G_{s,in}$ = 2.0 kg/m^2 s, the heat flux of the SHPi-HPo-2 surface is 1.7 times and 1.3 times that of HPo and HPi surfaces, respectively. The reason is that the gas-liquid interfacial shear stress increases with increasing steam mass fluxes, as discussed below.

During steam condensation process, flow directions of the steam and condensate liquid droplet/film are same. The shear stress on the gas-liquid interface increases with increasing steam

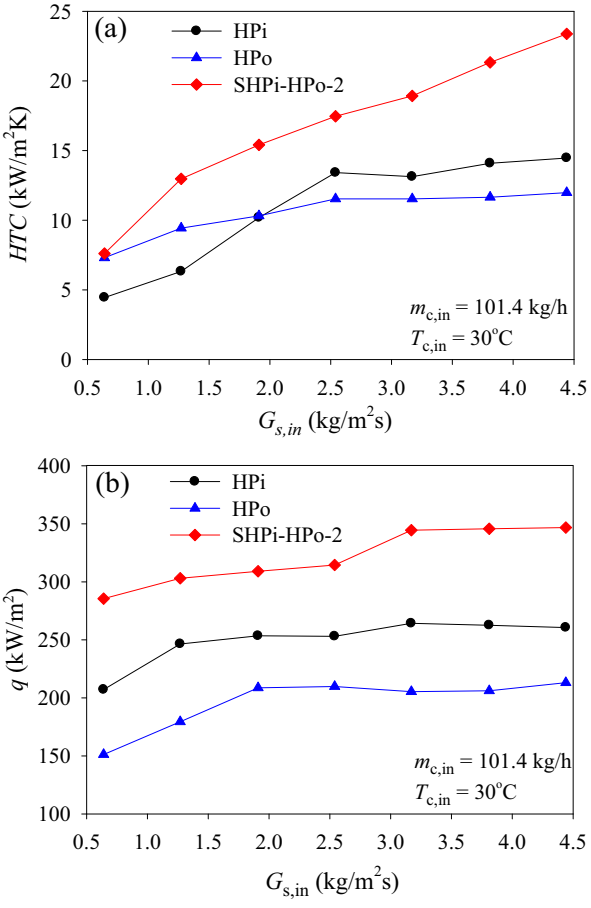

Fig. 8. Effects of steam mass flux on the condensation heat transfer.

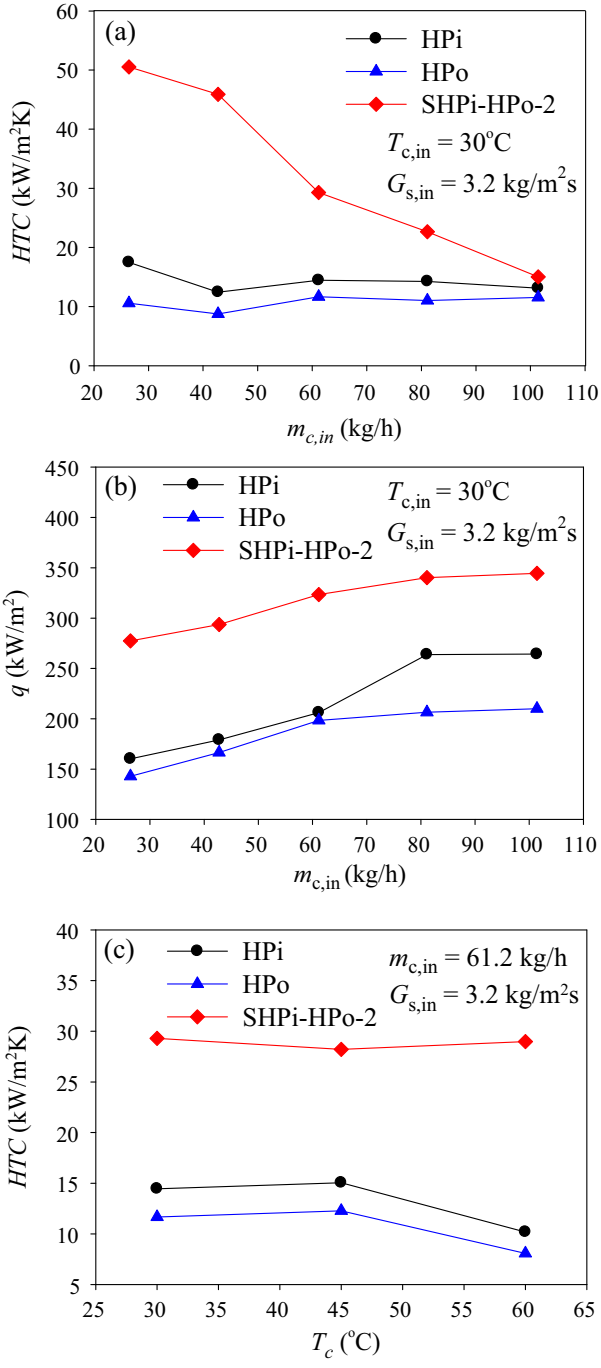

Fig. 9. Effects of cooling water mass flow rate and temperature on the condensation heat transfer.

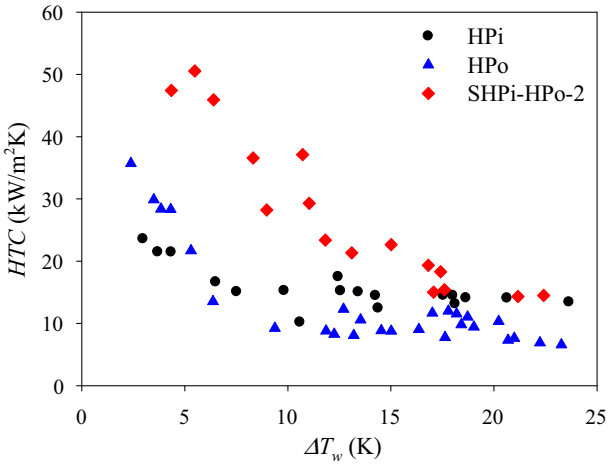

Fig. 10. Effects of wall subcooling on the condensation heat transfer.

mass fluxes, and accelerates the liquid droplet/film movement. Therefore, there is a proportional relationship between the steam mass fluxes and condensation heat transfer. Low steam mass fluxes causes shear force weakened, reduces the renewal speed of the liquid film for HPi surface. However, the liquid droplets grow slowly and keep smaller diameter on HPo surface at low steam mass fluxes, so the HPo surface has higher *HTC* than that of HPi surface. However, at high steam mass fluxes, the droplet growth rate on HPo surface was accelerated, the number of large droplet is increased. If a large amount of droplets cannot be separated from the surface in time, the heat resistance will be greatly increased. For HPi surface, large gas-liquid interfacial shear stress promotes the condensate film renewal speed at high steam mass fluxes. Therefore, although HPo surface can achieve droplet condensation on it, its *HTC* is still smaller than that of HPi surface at high mass fluxes. This conclusion is consistent with the literature [18].

3.4. Effects of cooling water mass flow rate and temperature

Fig. 9 shows the effects of cooling water mass flow rate and temperature on the condensation heat transfer. Five cooling water mass flow rates and three cooling water temperatures of 30 °C, 45 °C and 60 °C were selected. From Fig. 9a, we can see that the *HTC* of HPi and HPo surfaces change little with increasing cooling water mass flow rate, while the *HTC* of SHPi-HPo-2 surface decreases with increasing cooling water mass flow rate. With increasing cooling water mass flow rate, wall subcooling increases. Continuous liquid film will be formed in superhydrophilic grooves. Then, with the accumulation of liquid film, the liquid film in superhydrophilic grooves may diffuse to both sides of the hydrophobic surface, or even cover whole hydrophobic surface between two adjacent superhydrophilic grooves. The condensation heat transfer will become worse. At last, heat transfer enhancement gradually disappears for this hybrid surface. It is obvious for SHPi-HPo-2 surface that the heat transfer enhancement is large at low subcooling, and the heat transfer coefficient has the largest value among three surfaces. However, the heat transfer enhancement will disappears at high subcooling, and HTC is close to that of other two surfaces.

As observed in Fig. 9b, the heat fluxes increase gradually with increasing cooling water mass flow rate for three surfaces. At the same cooling water mass flow rate, the SHPi-HPo-2 surface has the largest q among three surfaces. As the cooling water mass flow rate reaches 80 kg/h, all the heat fluxes reach a stable value.

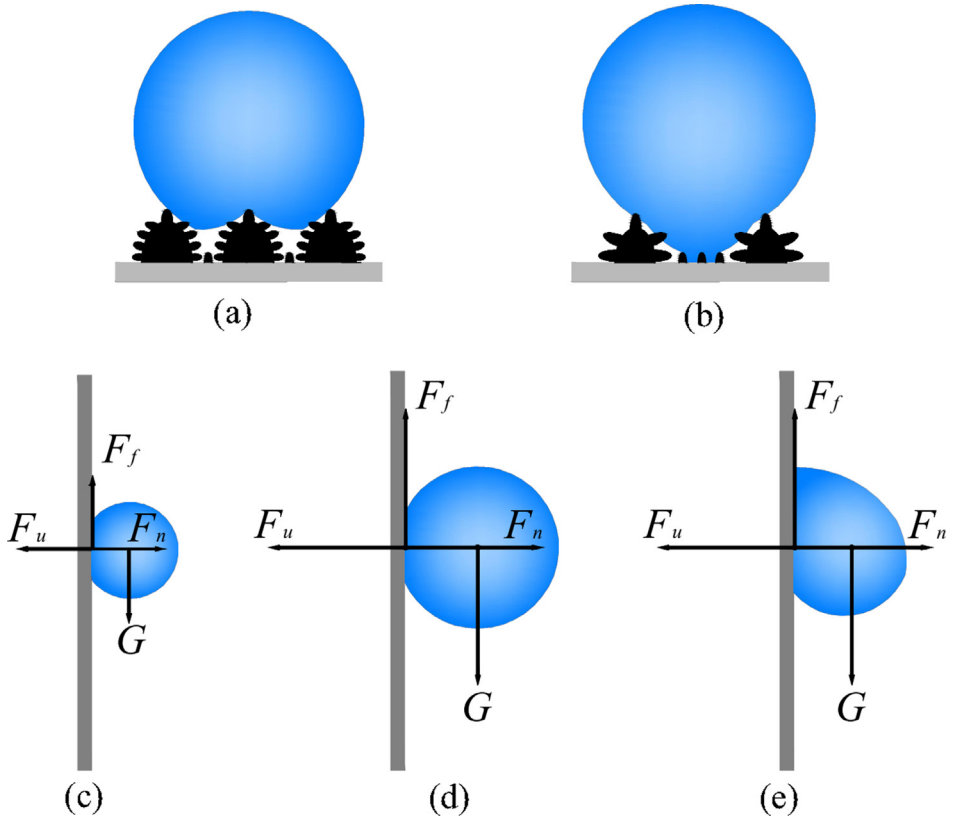

Fig. 11. Schematic diagram of a droplet on the surface and force analysis of a droplet on a vertical plate ((a) and (c) for low adhesion superhydrophobic surface, (b) and (d) for high adhesion superhydrophobic surface, (e) for high adhesion superhydrophobic surface where approaching/receding contact angles were taken into consideration).

Because under the same cooling water temperature and steam mass fluxes, although the increase in cooling water mass flow rate is beneficial to enhance heat transfer, it also increases the wall subcooling which decreases *HTC*. The final results are the combination effects of two factors above. The effects of water temperature on the condensation heat transfer can be seen in Fig. 9c. The *HTC* of HPi and HPo surfaces decrease slightly with increasing cooling water temperature at high cooling water temperature, but the *HTC* of SHPi-HPo-2 surface is almost not affected by it.

3.5. Comparison and analysis of condensation heat transfer

Fig. 10 shows the relationship between wall subcooling and condensation heat transfer coefficient. The *HTCs* of three surfaces all decrease with increasing wall subcooling, but For SHPi-HPo-2 surface, the *HTC* decreases rapidly at $\Delta T_w < 17$ °C, then tends to a stable value which is approximately equal to that of HPi surfaces under the same subcooling. For HPi and HPo surfaces, the turning point of the *HTC* tending to be stable is about $\Delta T_w = 10$ °C. For all wall subcooling degrees, SHPi-HPo-2 surface maintains the highest *HTC* among three surfaces.

In Fig. 10, most data ($\Delta T_w > 5$ °C) show that HTC of hydrophobic surface prepared by PTFE + micro-nano SiO_2 is obviously lower than HTC of hydrophilic surface, which consistent with previous literatures [42]. Only as $\Delta T_w < 5$ °C, *HTC* of HPo surface is higher than that of HPi surface. The reason why dropwise condensation heat transfer on HPO surface is not ideal is that low thermal conductivity of the PTFE retards the growth rate of droplet, especially at higher subcooling situation. However, if PTFE coating is very thin and uniform, this hydrophobic surface has a certain condensation heat transfer enhancement at low sub-cooling, as we did in this experiment (relative to copper and aluminum, thermal conductivity of stainless steel itself is not high). As surface undercooling is small, condensation droplets are located at the top of the nanostructure on hydrophobic surface, forming an air cushion between the bottom of droplet and the condensation surface. The smaller solid-liquid contact ratio reduces the energy dissipation of droplets, which is favorable for droplet merging and falling. The

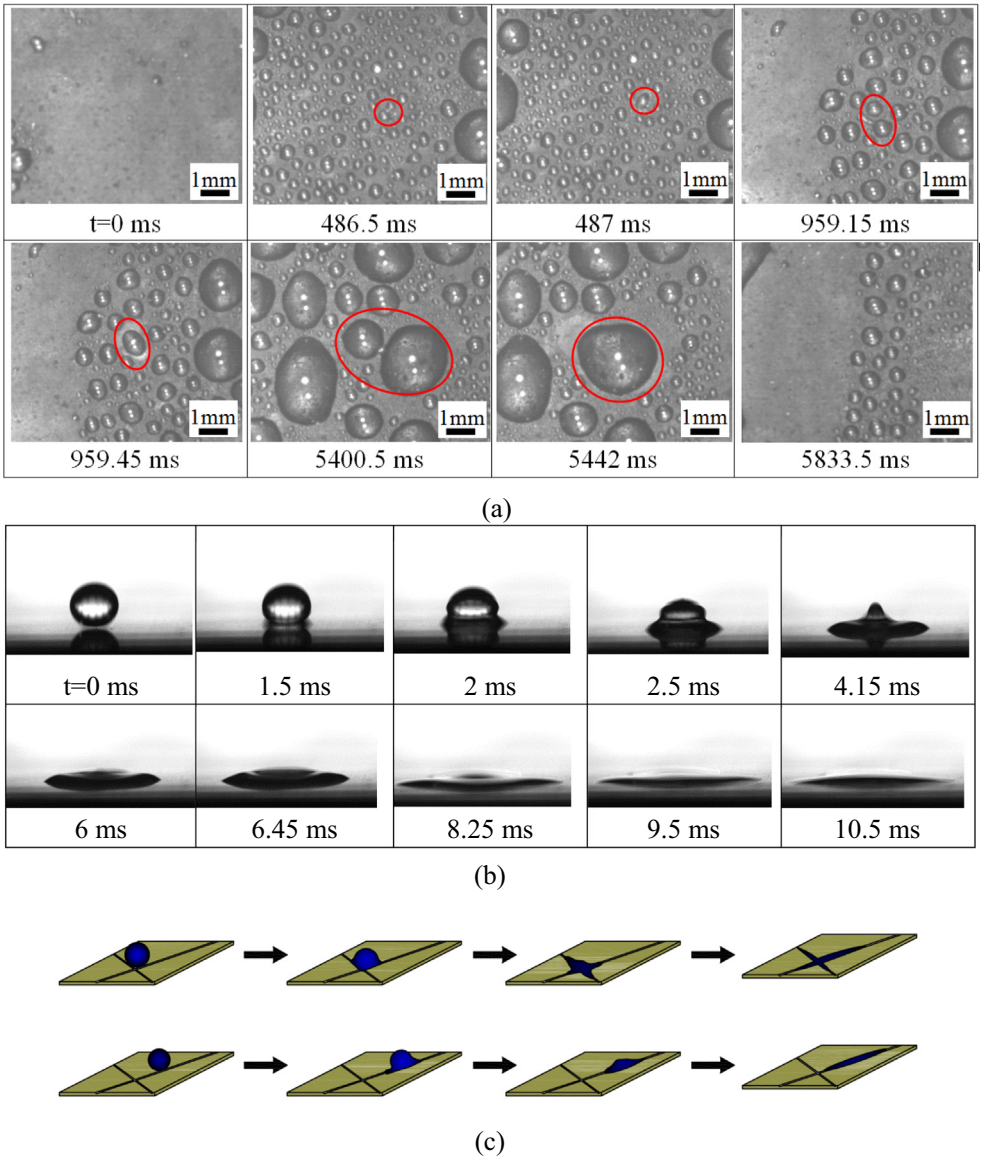

Fig. 12. (a) visualization of droplet growth and movement on HPo surface, (b) droplets spread on superhydrophilic surface, (c) a schematic diagram of droplet spreading and movement on SHPi-HPo surface.

average droplet size is small. With increasing surface subcooling, the depth of droplet penetration into the nanostructure increase, the adhesion work of droplet detachment increases, so droplet detachment diameter increases and the corresponding heat transfer coefficient decreases.

To achieve dropwise condensation, many researchers had prepared different condensation surface by modifying methods, including low adhesion superhydrophobic, high adhesion superhydrophobic and high adhesion hydrophobic surfaces etc. These surfaces can realize dropwise condensation very well. Some studies [43,44] found only the low adhesion surface has good condensation heat transfer performance, although both low and high adhesion superhydrophobic have approximately equal contact angle. Fig. 11a and b shows schematic diagrams of a droplet on the high and low adhesion superhydrophobic surfaces. In Fig. 11a, due to high density micro-nano structures on the low adhesion surface, droplet contact with solid surface belongs to "point contact", so the contact angle is large and the adhesion is low. In Fig. 11b, because of low density micro-nano structures and large gullies on the high adhesion superhydrophobic surface, droplet contact with solid surface belongs to "area contact", and the adhesion is high. Because of different values of adhesive forces, the balance of forces is different for droplets on the vertical surface. As shown in Fig. 11c, compared with high adhesion surface (see Fig. 11d), the low adhesion surface has a smaller adhesive force (F_u) to the droplet, so the support force (F_n) and friction force (F_f) also is smaller (according to the relationship between friction and support forces). If approaching/receding contact angles were taken into consideration, the contact area between the liquid droplet and the wall will increase at the same volume, so the effect of viscosity will increase. Also due to droplets deformation, the distance between the gravity center and the surface is shortened, that is, the gravitational moment is shortened, and the influence of gravity on the droplet rolling is reduced, as shown in Fig. 11e. In such a case, droplets must have larger diameters to detach from condensation wall. Thus for low adhesion superhydrophobic vertical surface, small diameter droplet can easily get out of it under the action of gravity. However, for high adhesion superhydrophobic vertical surface, the droplets do not detach from the surface until they grow into large enough. The large droplets are very unfavorable for the heat transfer enhancement. Therefore, in condensation heat transfer process, we need dropwise condensation with small droplets. At present, the low adhesion surface can achieve this goal, but the preparation technology is not perfect. When the low adhesion surface was scoured by high temperature steam for a period of time, it will not maintain the original characteristics of low adhesion and eventually become high adhesion superhydrophobic or high adhesion hydrophobic surface. This is also the reason why we put forward

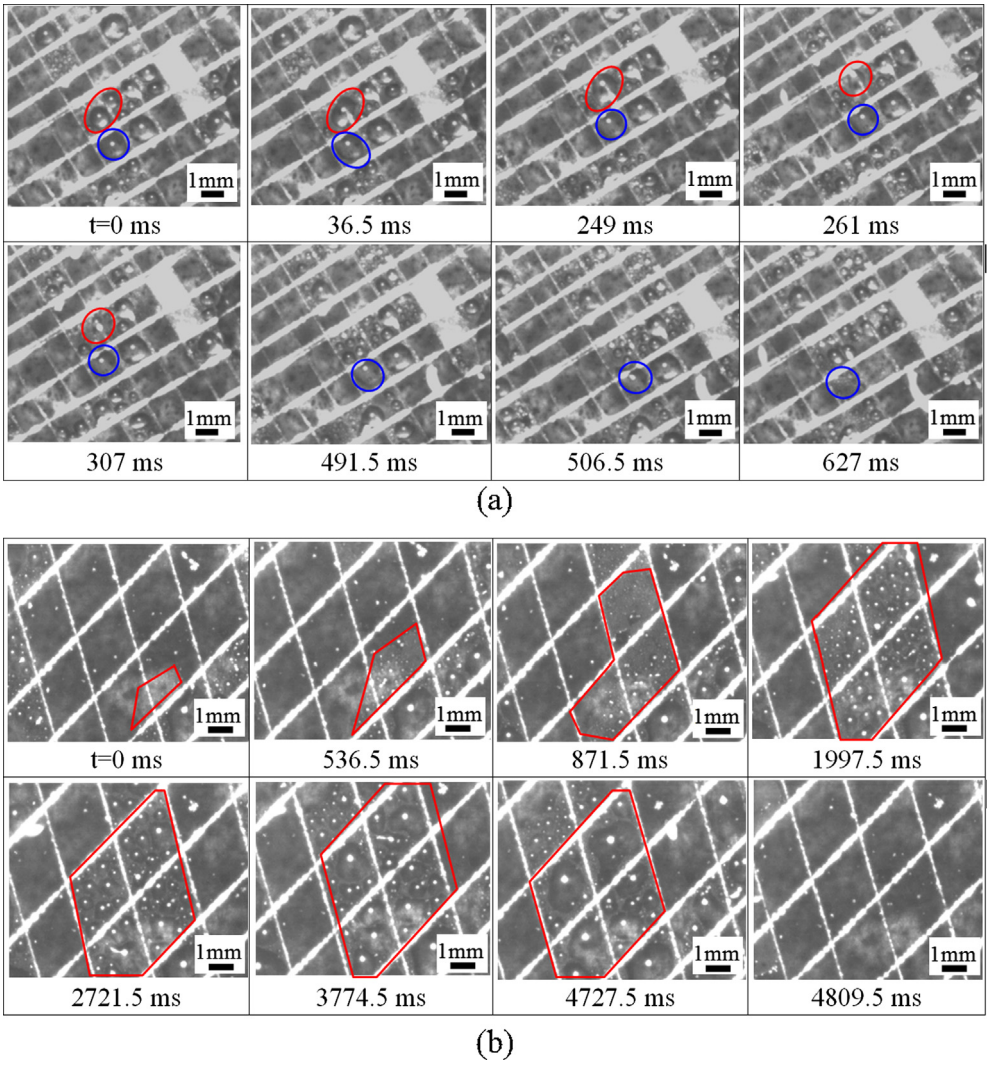

Fig. 13. Visualization of condensation process ((a) growth and movement of droplets on SHPi-HPo-1 surface, (b) droplet sweeping on SHPi-HPo-2 surface).

the superhydrophile-hydrophobic network hybrid surface to control droplet diameters.

Fig. 12a shows droplets are formed and detached periodically on HPo surface ($G_{s,in}$ = 3.2 kg/m^2 s, $T_{c,in}$ = 30 °C, $m_{c,in}$ = 101.4 kg/h). At t = 0 ms, large droplets have just completed detachment and leave a new blank place for formation and growth of new droplets. Then with the advance of time, new droplets gradually grow up and merge on the surface. Finally, droplets detach from the surface with a large diameter of 4.0 mm and take a long time to complete a cycle with a time of 5833.5 ms. To reduce droplet diameter and shorten droplet detachment cycle, the spreading characteristics of droplets on superhydrophilic surface can be used. As shown in Fig. 12b, when the droplets are exposed to a superhydrophilic surface, the droplets spread in a very short time, about 10.5 ms, which provide a way to limit the growth of large condensate droplets. The mechanism is shown in Fig. 12c. When the steam condenses and forms droplets on the hydrophobic region, the droplets grow, merge and move toward the superhydrophilic grooves (droplets can be located at different locations on the surface). Once the droplets contact the superhydrophilic grooves, the droplets are dragged rapidly by the superhydrophilic grooves. Then droplets spread in the groove in a very short time, which makes the droplets do not grow too large, being beneficial to strengthen condensation heat transfer.

For SHPi-HPo surface, we performed a visualization experiment to verify the control effects of hybrid surface on the droplet diameter, as shown in the Fig. 13a (for SHPi-HPo-1 surface, $G_{s,in}$ = 3.2 kg/m^2 s, $T_{c,in}$ = 30 °C, $m_{c,in}$ = 101.4 kg/h,). At t = 0 ms, two droplets (in red circle) begin to grow and close to superhydrophilic groove. At t = 36.5 ms, droplets touch the groove and merge into a large droplet. From t = 249 ms, the droplets begin to spread and the corresponding droplet diameter is reduced. Until t = 491.5 ms, droplets completely disappear from the field of vision, and a new droplet is generated at the location of original droplet. The time that a droplet last on SHPi-HPo surface in a cycle is far less than that on HPo surface. The droplet diameter on SHPi-HPo surface is about 1.0–1.5 mm which is less than 4.0 mm on HPo surface. This indicates that the SHPi-HPo surface have the ability of regulating droplet diameters and thereby enhancing condensation heat transfer. For the droplet (in blue[1] circle of Fig. 13a) below the groove, due to the resistance of gravity, it takes 625.0 ms to completely spread in the groove and disappear from the field of vision. Of course, in addition to the droplets being sucked away from hydrophobic region through superhydrophilic grooves, the droplets are swept away by other droplets which fall from top to down. As shown in Fig. 13b (SHPi-HPo-2 surface), at t = 0 ms, many small droplets appear on the surface, and then slowly grow up with time going on. Some droplets touching superhydrophilic grooves are sucked away and disappear. Some droplets between grooves begin to close superhydrophilic grooves. But at t = 4809.5 ms, the droplets was swept away before he was sucked into the superhydrophilic grooves. To sum up, For SHPi-HPo surface, there are two main ways to realize droplets detachment: being sucked away by superhydrophilic grooves and being swept away by other droplets.

3.6. Effects of grid spacing between grooves

Fig. 14 shows the effects of grid spacing between grooves on the condensation heat transfer. As shown in Fig. 14a, the *HTCs* of three surfaces gradually decrease with increasing wall subcooling. The SHPi-HPo-2 surface has the largest *HTC* at the same wall subcooling, reaching 50.5 kW/m^2 K. At ΔT_w = 9.0 K, the *HTC* of SHPi-HPo-2 surface are 1.2 and 1.7 times that of SHPi-HP-1 and SHPi-HP-3 surfaces, respectively. At high wall subcooling, the *HTCs* of three surfaces tend to be consistent. In Fig. 14b, the *HTC* of each surface increases with increasing steam mass flux. At $G_{s,\ in}$ = 3.17 kg/m^2 s, the *HTC* of SHPi-HP-2 surface is 1.4 and 1.6 times that of SHPi-HP-1 and SHPi-HP-3 surfaces, respectively. Obviously, the SHPi-HP-2 surface has the best condensation heat transfer performance in our experiments.

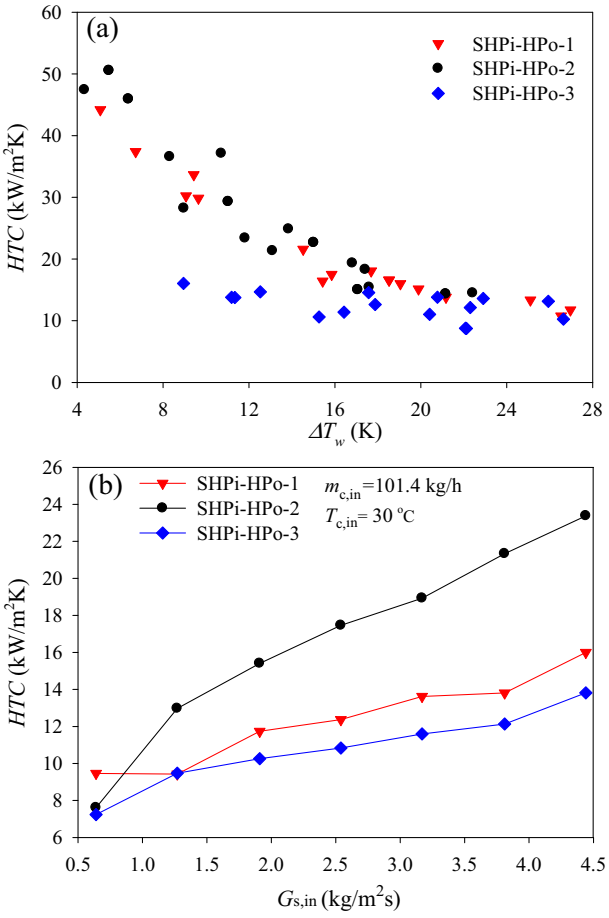

Fig. 14. Effects of grid spacing on the condensation heat transfer.

Using visualization results can explain the differences of condensation heat transfer for different surface. In Fig. 15a there is the largest droplet diameter on HPo surface and the smallest droplet diameter on SHPi-HPo-1 surface (Notice! We compare the largest droplet diameter on each surface). Among three SHPi-HPo surfaces, the average droplet diameter increases with increasing grid spacing. Does the SHPi-HPo-1 surface with the smallest droplet diameter have the best condensation heat transfer performance? The answer is no, because the heat transfer performance of the surface is not only related to the droplet diameter, but also related to the area percent of different droplets size and liquid film on the surface. Although the SHPi-HPo surface with small grid spacing can achieve small diameter droplets, temporary liquid film will be formed on this surface during the droplet sweeping process (see white region on the picture of SHPi-HPo-1 surface in Fig. 15a). The existence of the temporary liquid film affects the condensation heat transfer. So not the grid spacing as small as possible for achieving good condensation heat transfer performance and there is optimal grid spacing. In fact, the heat transfer is mainly through small droplets. Small diameter droplets are beneficial to the heat transfer, large diameter droplets and temporary liquid film formed between the grids will impede the heat transfer enhancement. The

[1] For interpretation of color in Fig. 13, the reader is referred to the web version of this article.

overall heat transfer results depend on the combination of these two aspects mentioned above. As shown in Fig. 15b ($G_{s,in}$ = 3.2 kg/m^2 s, $T_{c,in}$ = 30 °C, $m_{c,in}$ = 101.4 kg/h), we have counted the area percent distribution of deferent droplet diameter and temporary liquid film on each surface. Although there is no liquid film on HPo surface, the droplet diameter and area percent of the droplet diameter more than 1.2 mm (about 53.9%) are large. At the same time, HPo surface has the smallest area percent of droplets with a diameter less than 1.2 mm among four surfaces. Therefore, its condensation heat transfer performance is not good. For SHPi-HPo-3 surface, due to the large grid spacing between grooves, there is no liquid film on the surface and the area percent of droplets diameter more than 1.2 mm is 49%, the condensation heat transfer performance are somewhat similar to that of HPo surface. Although there is liquid film on SHPi-HPo-1 and SHPi-HPo-2 surface, the total area percent of liquid film and droplets with a diameter more than 2.3 mm is 39.6% and 23.4%, respectively, which is small. So the condensation heat transfer performance of SHPi-HPo-1 and SHPi-HPo-2 surface is better than that of HPo surface and SHPi-HPo-3 surface. For SHPi-HPo-2 surface, the area percent of large droplet and liquid film is small, and the area percent of droplets with a diameter less than 1.2 mm among four surfaces is the largest. While for SHPi-HPo-1 surface, the area percent of liquid film among four surfaces is the largest. Therefore, the heat transfer performance of SHPi-HPo-2 surface is the best and the SHPi-HPo surfaces are capable of controlling the droplet size and strengthening the condensation heat transfer. Of course, in present experiments, we only conduct heat transfer experiments on SHPi-HPo surfaces with three grid spacings and found the SHPi-HPo-2 surface has the best heat transfer performance. But on SHPi-HPo-2 surface there is still liquid film during the steam condensation process. Therefore, to further investigate the optimum grid spacing and superhydrophilic groove parameters is an important work in the future, it may make SHPi-HPo surfaces have the largest area percent of small droplet and no liquid film existence.

In fact, an ideal condensation surface should have the following characteristics: (1) possess as many nucleation sites as possible; (2) droplets rapidly nucleate and grow; (3) droplets rapidly detach from surface. However, the condensation process is complex. The more hydrophilic the surface is, the more conducive to the droplets nucleation, but not conducive to the droplet detachment. The thicker the liquid film is, the greater the thermal resistance. Therefore, simultaneously improving the droplets nucleation and detachment is the highlight of enhancing condensation heat transfer. In present experiments, superhydrophilic-hydrophobic network hybrid surface realize this purpose. But what is the best grid spacing? According to the formula below [45], the maximum droplet detachment diameter is

$$R_{\max} = \left(\frac{6c(\cos\theta_R - \cos\theta_A)\sin\theta}{\pi(2 - 3\cos\theta + \cos^3\theta)} \frac{\sigma_{lv}}{\rho_1 g} \right)^{1/2} \tag{9}$$

where coefficient c is related to the droplet contact line, θ is the static contact angle, σ_{lv} is vapor-liquid interface tension. Formula (9) shows that droplet detachment diameter is closely related to the dynamic and static contact angle. Therefore, the grid spacing should be determined according to the contact angle. In present experiments, the maximum droplets detachment diameter is 4 mm for HPo surfaces. Therefore, to reduce the droplets detachment diameter, the grid spacing should be smaller than the

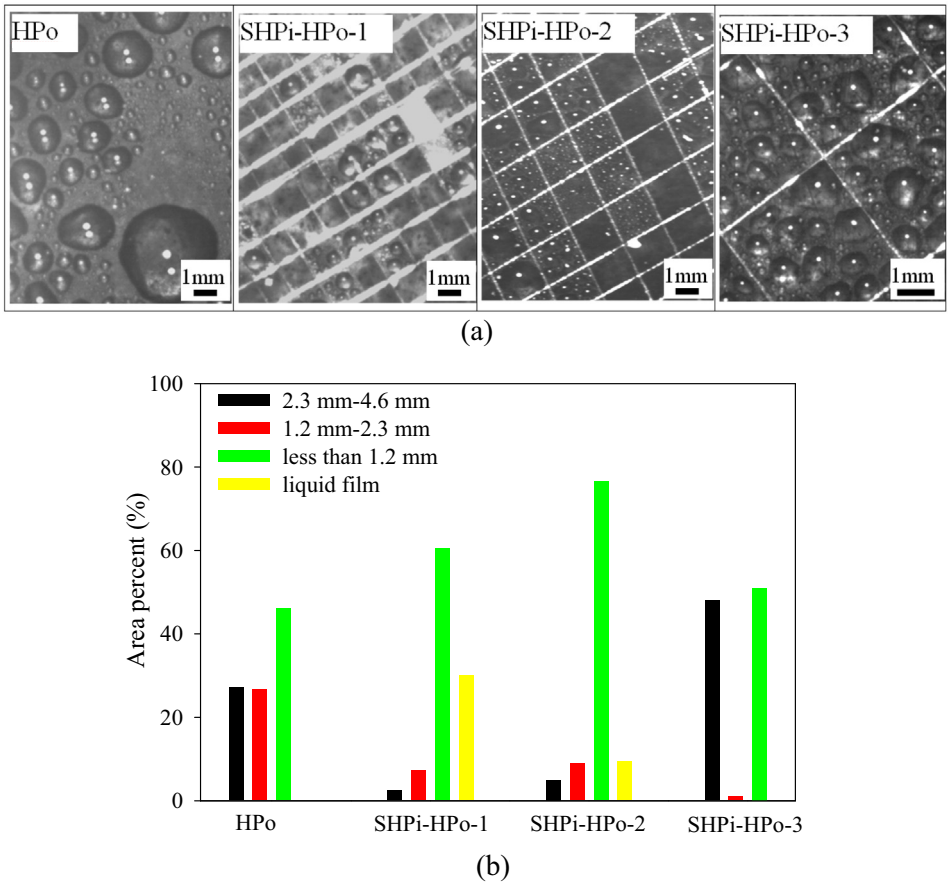

Fig. 15. (a) Pictures of droplets on four surfaces and (b) bar graph for area percent of droplets and liquid film.

maximum detachment diameter 4 mm. This is the reason why 1.5, 2.5 and 3.5 mm are selected for the experiments. When the grid spacing is 1.5, 2.5 and 3.5 mm, Bond number of droplets can be calculated by the following formula.

$$Bo = \frac{\left(\rho_l - \rho_g\right) g d^2}{\sigma_l} \tag{10}$$

The Bond number is 2.67 even for 1.5 mm grid spacing; this shows that the influence of gravity cannot be ignored. According to Young-Laplace formula $p_c = 2\sigma/R$, when droplets on hydrophobic region contact the superhydrophilic groove, both the hydrophobic region and the superhydrophilic groove will produce an additional pressure p_c driving droplets into the superhydrophilic groove from the hydrophobic region. On network hybrid surface, the average diameter of droplets is small, which will make the Bond number small. As the Bond number decreases, the surface tension plays a dominant role, the driving effect of the hydrophobic region and the superhydrophilic groove on the droplets is more obvious. Especially for small grid spacing surface, such as 1.5 mm grid spacing surface, continuous liquid film will be formed between two grooves and cover hydrophobic surface region, which hinder condensation heat transfer. Large grid spacing, such as 3.5 mm, is close to the actual maximum droplet detachment diameter. Droplets can be inhaled only close to the superhydrophilic grooves, so the droplet diameter is larger. On 2.5 mm grid spacing surface, the droplet diameter is small, although continuous liquid film was formed, the number is small. Therefore, this surface (2.5 mm grid spacing) has the best heat transfer performance.

4. Conclusions

The conclusions are summarized as follows:

(1) SHPi-HPo surfaces were proposed to enhance condensation heat transfer. These surfaces were prepared with fluorocarbon coating using PTFE as the matrix resin and micro-nano SiO_2 as additive to control surface roughness, which can withstand the scour of high temperature, has excellent physical and chemical properties.
(2) The heat transfer performance of SHPi-HPo surfaces is better than that of HPi and HPo surface. Superhydrophilic grooves are like a network on a background of HPo surface. It can suck away droplets timely and limit the growth of large condensate droplets. At ΔT_w = 6.3 K, the heat transfer coefficient of SHPi-HPo-2 surface is 2.7 and 3.4 times that of HPi and HPo surface, respectively.
(3) The SHPi-HPo surfaces can effectively control droplet diameter, but it's not that the smaller the grid spacing, the better the condensation heat transfer. When the grid spacing is too small, there is temporary liquid film occurred on the hybrid surface, which is not beneficial for the condensation heat transfer enhancement. There is optimum grid spacing between grooves to make surface have the best condensation heat transfer. In this paper, the SHPi-HPo-2 surface can achieve the largest area percent of small droplets and has the best heat transfer performance. In three SHPi-HPo surfaces, the heat transfer performance of SHPi-HPo-2 surface is 0–10% higher than that of SHPi-HPo-1 surface, and at ΔT_w = 9 K, the heat transfer coefficient is 1.7 times that of SHPi-HPo-3 surface.

Conflict of interest

The authors declared that there is no conflict of interest.

Acknowledgements

This work is supported by the National Natural Science Foundation of China (51676071), the Key Project of Natural Science Foundation of China (51436004).

References

[1] J.M. Beér, High efficiency electric power generation: the environmental role, Prog. Energy Combust. Sci. 33 (2) (2007) 107–134.
[2] A.D. Khawaji, I.K. Kutubkhanah, J.M. Wie, Advances in seawater desalination technologies, Desalination 221 (1) (2008) 47–69.
[3] P.R. Mashaei, M. Shahryari, S. Madani, Analytical study of multiple evaporator heat pipe with nanofluid; A smart material for satellite equipment cooling application, Aerosol Sci. Technol. 59 (2016) 112–121.
[4] T. Leonardi, M. Ishii, Condensation heat transfer with noncondensable gas for passive containment cooling of nuclear reactors, Nucl. Eng. Des. 236 (17) (2006) 1789–1799.
[5] C. Antonini, M. Innocenti, T. Horn, M. Marengo, A. Amirfazli, Understanding the effect of superhydrophobic coatings on energy reduction in anti-icing systems, Cold Reg. Sci. Technol. 67 (1–2) (2011) 58–67.
[6] B.J. Chung, M.C. Kim, M. Ahmadinejad, Film-wise and drop-wise condensation of steam on short inclined plates, J. Mech. Sci. Technol. 22 (2008) 127–133.
[7] I.S. Park, D.H. Choi, Heat- and mass-transfer analysis for the condensing film flow along a vertical grooved tube, Int. J. Heat Mass Transfer 44 (22) (2001) 4277–4285.
[8] P.S. Mahapatra, A. Ghosh, R. Ganguly, C.M. Megaridis, Key design and operating parameters for enhancing dropwise condensation through wettability patterning, Int. J. Heat Mass Transfer 92 (2016) 877–883.
[9] E. Schmidt, W. Schurig, W. Sellschopp, Versuche über die Kondensation von Wasserdampf in Film und Tropfenform, Technische Mechanik Und Thermodynamik 1 (2) (1930) 53–63.
[10] J.W. Rose, Dropwise condensation theory and experiment: a review, P. I. Mech. Eng. A-J. Pow. 216 (2) (2005) 115–128.
[11] B.S. Sikarwar, S. Khandekar, S. Agrawal, S. Kumar, K. Muralidhar, Dropwise condensation studies on multiple scales, Heat Transfer Eng. 33 (4–5) (2012) 301–341.
[12] F. Chu, X. Wu, Fabrication and condensation characteristics of metallic superhydrophobic surface with hierarchical micro-nano structures, Appl. Surf. Sci. 371 (2016) 322–328.
[13] R. Wen, S. Xu, D. Zhao, Y.C. Lee, X. Ma, R. Yang, Hierarchical superhydrophobic surfaces with micropatterned nanowire arrays for high-efficiency jumping droplet condensation, Acs Appl. Mater. Inter. 9 (51) (2017) 44911.
[14] R.D. Narhe, D.A. Beysens, Water condensation on a super-hydrophobic spike surface, Epl. 75 (1) (2006) 98–104.
[15] K.W. Kim, C.D. Sang, J.S. Ko, H.J. Ji, Observation of water condensate on hydrophobic micro textured surfaces, Heat Mass Transfer 49 (7) (2013) 955–962.
[16] K.W. Hwang, D.H. Kim, H.J. Jo, H.S. Park, K. Moriyama, M.H. Kim, Effects of heat flux on dropwise condensation on a superhydrophobic surface, J. Mech. Sci. Technol. 30 (5) (2016) 2141–2149.
[17] S. Lee, K. Cheng, V. Palmre, M.D. Mainul Hossain Bhuiya, K.J. Kim, Heat transfer measurement during dropwise condensation using micro/nano-scale porous surface, Int. J. Heat Mass Transfer 65 (7) (2013) 619–626.
[18] X.M. Chen, J. Wu, R.Y. Ma, M. Hua, N. Koratkar, S.H. Yao, Z.K. Wang, Nanograssed micropyramidal architectures for continuous dropwise condensation, Adv. Funct. Mater. 21 (24) (2015) 4617–4623.
[19] C. Yamali, H.M. Jr, A theory of dropwise condensation at large subcooling including the effect of the sweeping, Heat Mass Transfer 38 (3) (2002) 191–202.
[20] B.S. Sikarwar, N.K. Battoo, S. Khandekar, K. Muralidhar, Dropwise condensation underneath chemically textured surfaces: simulation and experiments, J. Heat Transfer 133 (2) (2011) 216–226.
[21] P.M. Somwanshi, K. Muralidhar, S. Khandekar, Dropwise condensation patterns of bismuth formed on horizontal and vertical surfaces, Int. J. Heat Mass Transfer 122 (2018) 1024–1039.
[22] M.K. Chaudhury, G.M. Whitesides, How to make water run uphill, Science 256 (5063) (1992) 1539.
[23] X. Zhu, H. Wang, Q. Liao, Y.D. Ding, Y.B. Gu, Experiments and analysis on self-motion behaviors of liquid droplets on gradient surfaces, Exp. Therm. Fluid Sci. 33 (6) (2009) 947–954.
[24] A.M. Macner, S. Daniel, P.H. Steen, Condensation on surface energy gradient shifts drop size distribution toward small drops, Langmuir 30 (2014) 1788–1798.
[25] B.L. Peng, X.H. Ma, Z. Lan, R. Wen, Experimental investigation on steam condensation heat transfer enhancement with vertically patterned hydrophobic-hydrophilic hybrid surfaces, Int. J. Heat Mass Transfer 83 (2015) 27–38.
[26] Q. Guo, P. Cheng, 3D lattice Boltzmann investigation of nucleation sites and dropwise-to-filmwise transition in the presence of a non-condensable gas on a biomimetric surface, Int. J. Heat Mass Transfer 128 (2019) 185–198.
[27] J.B. Boreyko, C.H. Chen, Self-propelled dropwise condensate on superhydrophobic surfaces, Phys. Rev. Lett. 103 (18) (2009) 184501.

[28] J. Feng, Z.Q. Qin, S.H. Yao, Factors affecting the spontaneous motion of condensate drops on superhydrophobic copper surfaces, Langmuir 28 (14) (2012) 6067–6075.
[29] B.L. Peng, S.F. Wang, Z. Lan, W. Xu, R.F. Wen, X.H. Ma, Analysis of droplet jumping phenomenon with lattice Boltzmann simulation of droplet coalescence, Appl. Phys. Lett. 102 (15) (2013) 151601.
[30] R.N. Leach, F. Stevens, S.C.L. And, J.T. Dickinson, Dropwise condensation: experiments and simulations of nucleation and growth of water drops in a cooling system, Langmuir 22 (21) (2006) 8864–8872.
[31] F.Q. Chu, Z.P. Yuan, X. Zhang, X.M. Wu, Energy analysis of droplet jumping induced by multi-droplet coalescence: the influences of droplet number and droplet location, Int. J. Heat Mass Transfer 121 (2018) 315–320.
[32] C. Yamali, J.H. Merte, Influence of sweeping on dropwise condensation with varying body force and surface subcooling, Int. J. Heat Mass Transfer 42 (15) (1999) 2943–2953.
[33] C. Yamali, H.J. Merte, A theory of dropwise condensation at large subcooling including the effect of the sweeping, Heat Mass Transfer 38 (2002) 191–202.
[34] M. Izumi, S. Kumagai, R. Shimada, N. Yamakawa, Heat transfer enhancement of dropwise condensation on a vertical surface with round shaped grooves, Exp. Therm. Fluid Sci. 28 (2–3) (2004) 243–248.
[35] Y.A. Lee, L.S. Kuo, T.W. Su, C.C. Hsu, P.H. Chen, Orientation effects of nanoparticle-modified surfaces with interlaced wettability on condensation heat transfer, Appl. Therm. Eng. 98 (2016) 1054–1060.
[36] A.B. Kananeh, M.H. Rausch, A.P. Fröba, A. Leipertz, Experimental study of dropwise condensation on plasma-ion implanted stainless steel tubes, Int. J. Heat Mass Transfer 49 (25–26) (2006) 5018.
[37] A.R. Parker, C.R. Lawrence, Water capture by a desertbeetle, Nature 414 (2001) 33–34.
[38] J. Ju, H. Bai, Y. Zheng, T. Zhao, R. Fang, L. Jiang, A multi-structural and multi-functional integrated fog collection system in cactus, Nat. Commun. 3 (4) (2012) 1247.
[39] J. Xie, J. Xu, Y. Cheng, F. Xing, And, X He, Condensation heat transfer of R245fa in tubes with and without lyophilic porous-membrane-tube insert, Int. J. Heat Mass Transfer 88 (2015) 261–275.
[40] A. Bisetto, S. Bortolin, D.D. Col, Experimental analysis of steam condensation over conventional and superhydrophilic vertical surfaces, Exp. Therm. Fluid Sci. 68 (2015) 216–227.
[41] G.F. Hewitt, G.L. Shires, T.R. Bott, Process Heat Transfer, CRC Press Inc., Boca Raton, FL, 1994.
[42] B.J. Zhang, K. Cheng, K.J. Kim, T. Hwang, H. Yoon And, Dropwise steam condensation on various hydrophobic surfaces: polyphenylene sulfide (PPS), polytetrafluoroethylene (PTFE), and self-assembled micro/nano silver (SAMS), Int. J. Heat Mass Transfer 89 (2015) 353–358.
[43] T.Q. Liu, W. Sun, X.Y. Sun, H.R. Ai, Mechanism study of condensed drops jumping on super-hydrophobic surfaces, Colloid. Surf. A: Physicochem. Eng. Asp. 414 (46) (2012) 366–374.
[44] J. Feng, Y. Pang, Z. Qin, S. Yao, Why condensate drops can spontaneously move away on some superhydrophobic surfaces but not on others, Acs Appl. Mater. Inter. 4 (12) (2012) 6618–6625.
[45] S. Kim, K.J. Kim, Dropwise condensation modeling suitable for superhydrophobic surfaces, ASME J. Heat Transfer 133 (2011) 081502–081510.